

Origin of Jahn-Teller distortions in d-electron ABX_3 perovskites

J. Varignon¹, M. Bibes¹ and Alex Zunger²

¹*Unité Mixte de Physique, CNRS, Thales, Université Paris Sud, Université Paris-Saclay, 91767, France*

²*Energy Institute, University of Colorado Boulder Colorado 80309, Boulder, CO, USA*

Compounds with the ABX_3 perovskite structure ($X=F$ or O), where B is a $3d$ transition metal element, have fascinated the solid-state physics and chemistry communities for decades due to their broad range of properties and functionalities, encompassing magnetism, superconductivity or colossal magnetoresistance. A frequent phenomenon behind many of these properties is the Jahn-Teller distortion (JTD) that removes electronic degeneracies in partially occupied states and results in systematic, compound-dependent atomic displacements, orbital ordering and metal-insulator transitions. Here we analyze the driving forces behind the Jahn-Teller motions and associated electronic fingerprints in a full range of ABX_3 compounds. We find that space and spin symmetry broken density functional supercell theory explain the full trends in the experimental data without the need to introduce dynamic correlations. We identify systems prone to JTD and the relevant mode symmetry by nudging the orbital occupations of degenerate states in ideal cubic supercells, and observing those that lower the total energy by creating unequal occupations of the different degenerate partners. We identify (i) compounds that are prone to such electronically-driven instabilities (*i.e.* a pure JT effect) such as $KCrF_3$, $KCuF_3$, $LaVO_3$, $KFeF_3$ and $KCoF_3$, and proceed to relax the structures, finding quantitatively the JTD in excellent agreement with experiment; (ii) compounds such as $LaMnO_3$ or $LaTiO_3$ that do not show electronically driven JTD despite orbital degeneracies, because their strongly hybridized $B, d - X, p$ states supply but too weak JT forces to overcome the needed atomic distortions; (iii) although $LaVO_3$ exhibits similar $B, d - X, p$ hybridizations as $LaTiO_3$, the former compound exhibits a robust electronic instability while $LaTiO_3$ has zero stabilization energy, the reason being that $LaVO_3$ has two electrons t_{2g}^2 relative to $LaTiO_3$ with just one t_{2g}^1 . (iv) We explain the trends in “orbital ordering” whereby electrons occupy orbitals that point to orthogonal directions between all nearest-neighbor $3d$ atoms. Our results agree with different experimental observations on ABX_3 materials displaying electronic degeneracies. We thereby provide a unified vision to explain octahedra deformations in perovskites that, at odds with common wisdom, does not require the celebrated strong dynamically correlated vision of electron interactions codified by the Mott-Hubbard mechanism.

I. Introduction

ABX_3 ($X=O, F$) perovskites^{1,2} show a number of systematic atomic distortions relative to the ideal structure made of vertically positioned, all parallel BX_6 octahedra with equal B-X bonds. The interpretation of much of the electronic and magnetic phenomenology surrounding such perovskites^{1,2}, including superconductivity, colossal magnetoresistance or metal-insulator transitions is intimately related to the nature of the *causes and consequences* of the observed atomic distortions. The common view is that (i) the octahedral rotation and tilt such as in-phase ϕ_z^+ and anti-phase ϕ_z^- (ORT; displayed in Fig1.a, b) are a consequence of the classic *size mismatch* between the A, B, and X atoms, as reflected by geometrical packing constructs such as the Goldschmidt tolerance factor³, whereas (ii) the Jahn-Teller distortion (JTD)^{4,5} reflects an *electronic instability* associated with partial occupation of degenerate states⁶. Usually, JTD in ABX_3 perovskites produce inequivalent B-X bonds length, such as the Q_2 motion (*cf.* Figure 2 of Ref.⁵) that differentiate bond length along the x and y directions. These exist either as in-phase motions in consecutive planes along the z-axis (here labelled Q_2^+ motion, Fig1.c) or as in anti-phase along -z (here labelled Q_2^- motion, Fig1.d). However, it is not clear which of the observed distortions are electronically induced and which are purely steric. Understanding predictively the causes of the observed displacements is central to interpreting numerous related phenomena *e.g.* gap formation due to symmetry lowering, metal-insulator transitions⁷, “orbital-orderings”⁸⁻¹⁰ and magnetic interactions¹¹ in ABX_3 perovskites. This is important since controlling octahedral deformations by using temperature, ferroelectricity, strain engineering or heterostructures¹²⁻¹⁸, may offer much needed knobs to control electronic devices.

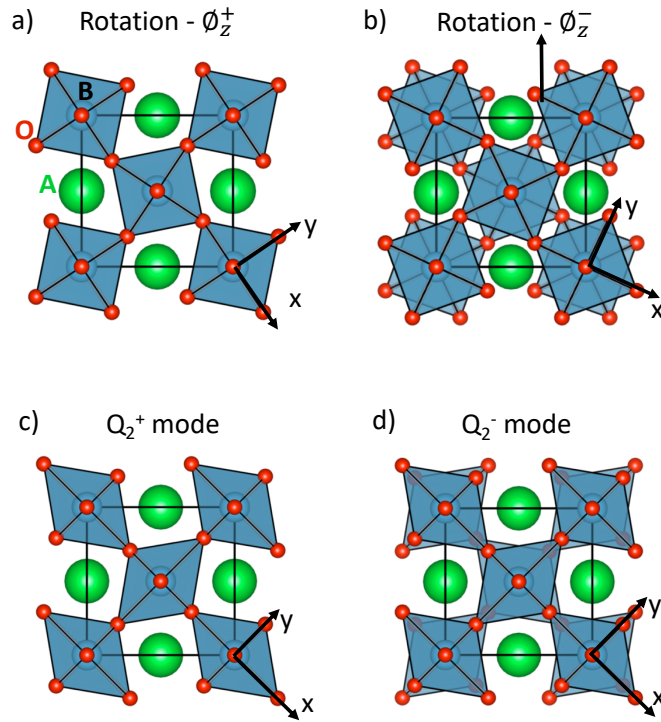


Figure 1: Sketches of the key lattice distortions appearing in ABX_3 materials. a and b) In phase (ϕ_z^+ , a) and anti-phase (ϕ_z^- , b) octahedral rotations around the z axis. c and d) Octahedral deformations propagating in phase (Q_2^+ , c) or in anti-phase (Q_2^- , d) along the z axis.

Predictive understanding of the mechanisms of octahedral distortions is rather challenging, for a number of reasons: (a) Compounds with the same degenerate configurations such as $KCrF_3$ ¹⁹, $KCuF_3$ ²⁰ and $LaMnO_3$ ²¹ being all e_g^1 ; or YVO_3 and $LaVO_3$ being both t_{2g}^2 (Ref. ²²) show different types of octahedral deformations at low temperature: Q_2^- for $KCrF_3$, $KCuF_3$ or $LaVO_3$, and Q_2^+ for YVO_3 and $LaMnO_3$, raising the question of what creates Q_2^+ and what creates Q_2^- ; (b) Recent theoretical works predicted the surprising appearance of strong in-phase Q_2^+ symmetry-lowering octahedral deformations in compounds such as $SrTiO_3$, $BiFeO_3$ or $BaMnO_3$ even when there are no degenerate states^{14,23}; (c) The textbook depiction of the JT force is often based on calculations based on the degenerate *orbital alone*, but one must consider the force resulting from the systems total energy, including not only the sum of one-electron orbital energy but also the electron-electron Coulomb and exchange-correlation energies resulting from degeneracy removal. (d) Finally, literature models for explaining the origin of octahedral deformations in ABX_3 materials span a large range of mechanisms, including electronic super-exchange (Kugel-Khomskii model)^{24,25}, electron-phonon coupling^{9,26}, lattice mode couplings involving rotations and forcing the Q_2^+ mode

^{13,27,28}, or specific dynamical correlation effects ^{29,30}. Since none of these proposed models has been applied to a full range of ABX₃ compounds with different e_g-like and t_{2g}-like orbital occupations, at this time it is not clear if different mechanisms are needed to explain different distortions in different compounds, or if there is a basic theoretical framework that could explain them all.

The often-voiced view that ABX₃ perovskites with B=3d element are strongly dynamically correlated systems has been reflected also in the context of understanding the octahedral deformations atomic displacements. For example, it has been suggested ²⁷ that *“LDA+U cannot describe the properties of LaMnO₃ at T>T_{Néel} and, in particular, at room temperature, where LaMnO₃ is a correlated paramagnetic insulator with a robust Jahn-Teller distortion”*. A similar statement for LaMnO₃ has been made in Ref.⁹: *“To identify the driving mechanism for orbital order in LaMnO₃, it is thus mandatory to account for both the realistic electronic structure and many-body effects”*. Similar statements have also been applied to fluorine based compounds such as KCuF₃³⁰: *LDA and GGA “usually fail to predict the correct electronic and structural properties of materials where electronic correlations play a role. Extensions of LDA, e.g., LDA + U and self-interaction correction LDA, can improve the results, e.g., the band gap value and local moment, but only for solids with long-range order. Hence the computation of electronic, magnetic, and structural properties of strongly correlated paramagnetic materials remains a great challenge.”* In this highly correlated view, gapping of Mott insulators occurs due to electron-electron interaction in the ideal undistorted octahedra, and symmetry breaking deformations can occur afterwards as a secondary fact. If correct, this view might suggest that the theoretical understanding of JTD and the effects related to it in ABX₃ materials would require the heavy computational machinery such as dynamic mean field theory and beyond. These literature statements raise the question of *what is the true minimal theoretical framework needed to capture the basic trends in octahedral atomic distortions across the ABX₃ series is and whether such symmetry lowering distortions are an integral part of explaining the electronic structure.*

We address this subject by using mean field like Bloch periodic DFT band theory with two stipulations. First, a polymorphous representation of the real space structure that permits the existence of different local environments to atoms and spins is required. This entails using

crystallographic cells that are not limited to the smallest primitive cell, and therefore allow orbital, spatial and spin symmetry breaking, should these modes lower the total energy. Second, breaking orbital symmetries of degenerate partners requires an exchange correlation functional that distinguishes occupied from unoccupied states, thereby affording significant cancellation of the self-interaction error and thus spatial compactness of 3d orbitals. Here we use DFT+U, (but nonzero U is not essential, as other exchange correlation functional make no use of an explicit U term³¹). This approach provides DFT with a fair opportunity to reveal if the different patterns of symmetry breaking—spin order; JTD and /or ORT, and orbital occupation symmetry breaking—lower the energy or not, thereby establishing a first-principles framework for predictive theory of displacements in ABX₃ perovskites.

To determine if a potential deformation has electronic origin we use a Landau-esque perturbation-induced symmetry lowering of an initially high symmetry cubic cell, and examine the total energy for (a) assumed equal occupations of the degenerate partners [such as (1/2, 1/2) for a single electron in doubly occupied e_g level] and (b) Orbital Broken Symmetry (OBS) of degenerate partners, looking for energy lowering occupation patterns *e.g.* (1, 0). If (b) gives total energy lowering relative to (a) this signals the propensity for an electronic instability in the parent high symmetry phase, which is then followed up by the complete relaxation of the unit cell displacements, providing our predicted JTD (possibly with coupling to ORT). If the unequal occupations configuration (b) returns to the equal occupation configuration (a) during self-consistent calculation, this indicates that the high symmetry system is electronically stable and thus not prone to develop an *electronically enforced* distortion. Distortions present may reflect other factors such as the classic steric effects induced by size mismatch. The main conclusions are:

(a) Perturbing in DFT the high symmetry cubic phase discloses which compounds tend to develop electronic instabilities and which do not: The existence of electronic instabilities, *i.e.* a JT effect, is predicted in the high symmetry Pm-3m cubic phase of several ABX₃ compounds (KCrF₃, KCuF₃, LaVO₃, KFeF₃ and KCoF₃) but other compounds such as LaMnO₃ or LaTiO₃ have no such instability.

(b) Instabilities are manifested by breaking of orbital degeneracies while lowering the total energy, and thereby concomitantly opening finite band gaps.

(c) “Orbital-ordering” is found to be a total energy lowering event. In such a state, electrons occupy an orbital that is pointing to orthogonal directions between all nearest-neighbor 3d atoms, such as alternation of d_{xy}/d_{yz} orbitals for a material with a t_{2g} degeneracy or alternation of d_y^2/d_x^2 orbitals for a material with an e_g level degeneracy.

(d) LaMnO_3 does not exhibit JTD whereas KCrF_3 does, despite isovalent ($t_{2g}^3 e_g^1$) configurations (and similarly for the t_{2g}^1 configuration LaTiO_3 has no JTD, whereas KFeF_3 does) because the existence of strong hybridization in the oxide cases which diminishes orbital localization needed to create JTD.

(e) Although LaVO_3 exhibits similar B, d – X, p hybridizations as LaTiO_3 , the former compound exhibits a robust electronic instability in the cubic cell while LaTiO_3 has zero stabilization energy, the reason being that LaVO_3 has two electrons t_{2g}^2 relative to LaTiO_3 with just one t_{2g}^1 . We also find that the JTE has a subtle interplay with octahedra rotations, cooperating for t_{2g}^2 materials, thereby offering a valuable knob to tune the JTE temperature.

(f) The Q_2^- octahedral deformation mode is a Jahn-Teller distortion: Following the identification of electronic instabilities in cubic cells, we follow the quantum mechanical forces to establish the fully relaxed crystal structures, finding that the aforementioned JTD compounds develop a Q_2^- octahedra deformation mode, which is therefore identified as an electronically induced Jahn-Teller distortion and the fingerprint of a Jahn-Teller effect. The significance of the development of this specific Q_2^- mode is that it is characterized by *opposite* octahedral deformations between nearest sites and is thus able to accommodate orbital-ordering. Calculation of the magnitude of the displacements shows good agreement with the experimentally observed trends in a full range of ABX_3 compounds with t_{2g} and e_g degenerate partners. Furthermore, the tetragonal-to-monoclinic phase transition observed in KCrF_3 originates from steric effects and does not imply any strong, dynamic, electronic correlation effects.

(g) The other Q_2^+ octahedral deformation, appearing in LaMnO_3 or LaTiO_3 , is not induced by an electronic instability and thus it is not a Jahn-Teller distortion. It is a consequence of octahedral rotations and tilts often appearing in the perovskite oxides due to pure geometric steric effects. The Q_2^+ octahedral deformation mode thus cannot signal strong dynamical correlation effects in these ABX_3 compounds. Also, the “consequence of octahedra rotations” origin of the Q_2^+ motion is confirmed by experiments on LaMnO_3 .

We conclude that the electronically-induced Jahn-Teller distortion mode Q_2^- and the geometrically induced steric Q_2^+ octahedral deformation mode are fully captured by a static mean-field method. This is in line with recent theoretical works that have demonstrated that static mean-field methods capable of inducing broken symmetry such as Density Functional Theory^{13,27,31,32} in a polymorphous representation suffice to also explain (i) the trends in gapping and type of magnetic order across the ternary ABO_3 series³² and the binary 3d oxide series^{33,34}; (ii) the trends in disproportionation into two different local environments of the B site $2ABO_3 \rightarrow A_2[B,B']O_6$ ³⁵ and (iii) the explanation of doping Mott insulators including cuprates^{36,37}, doping Kagome structures³⁸ as well as “anti-doping” oxides³⁹.

II. Methods

The main features of the theoretical framework used in the study are as follows:

(a) Cell geometry and relaxation: We consider the following structure types: high symmetry Pm-3m cubic cell (LaTiO₃, LaVO₃, LaMnO₃, KFeF₃, KCoF₃, KCrF₃ and KCuF₃) as well as the experimentally observed structures, namely I_4/mcm (KCuF₃, KCrF₃), $Pbnm$ (LaTiO₃, LaVO₃, LaMnO₃, LaTiO₃), $P2_1/b$ (LaVO₃), I_2/m (KCrF₃), $P-1$ (KCoF₃) and I_2/a (KFeF₃) for identifying the DFT ground state structure. We allow cell sizes larger than the minimal (one formula unit per cell) so as to permit symmetry breaking distortions, should they lower the total energy. Atoms have to be nudged initially off their high symmetry positions in the cubic cell, followed by the calculation of the restoring Hellman Feynman forces guiding full relaxation. In order to provide sufficient flexibility for developing general patterns of energy lowering deformations we have used a polymorphous crystallographic cell corresponding to a $(\sqrt{2}a, \sqrt{2}a, 2a)$ cubic cell (*i.e.* 4 f.u per cell). The structural relaxation (lattice parameters and atomic positions) of ground state structures has also been performed until forces are lower than 1 meV/Å. We performed a symmetry adapted mode analysis that allows to extract the amplitudes of general distortion modes by projecting the distorted structure on the basis of the phonon eigen-displacements of the high symmetry cubic cell^{40,41}.

(b) Orbital symmetry breaking: The occupation numbers of partially filled degenerate orbitals in the high symmetry cubic cell is not restricted to equal occupations of the degenerate partners. For a compound with a single e_g electron, we do not pre-select a (1/2,

1/2) occupation pattern as generally done in standard band calculations, but allow also exploration of a (1,0) occupation pattern. Analogously, for 2 electrons in the t_{2g} level we explore (2/3, 2/3, 2/3) vs. (1,1,0) occupation patterns. Wave function symmetrization to a presumed symmetry is avoided so as to allow electrons to freely occupy energy lowering configurations. We therefore initially nudge not only atomic positions but also the occupation patterns of electrons in specific degenerate partners, called orbital broken symmetry states (OBS)^{42–44}. The self-consistent field with possible changes in d orbital occupancies is then obtained starting from this initial guess.

(c) Spin order: We use the observed low temperature spin order, *e. g.* AFM-A (ferromagnetic planes coupled antiferromagnetically together), AFM-C (AFM planes coupled ferromagnetically together) and AFM-G (all nearest neighbor cations are antiferromagnetically coupled). For the study of the linear response of the ideal cubic phase, we used a simple FM order so as to avoid a strongly entangled spin-orbital situation^{24,45}. Since we have previously shown that low temperature spin-ordered phase inherits the physics of the high temperature PM phase in ABO_3 materials³² we did not attempt to model the PM distortions presently. This is reinforced by experimental observations of octahedra deformations appearing at higher temperatures than the AFM to PM (for example, in $KCrF_3$, $KCuF_3$, $LaMnO_3$).

(d) Exchange-correlation functional: To enable energy lowering occupations one needs to use an exchange-correlation (XC) functional that distinguishes occupied from unoccupied states. Local (LDA) and semi-local (GGA, meta-GGA) XC functionals do not make such distinction. The simplest XC allowing this is DFT+U, where U is an on-site potential acting on a subset of orbitals – here the transition metal (TM) d states – and shifting to lower (upper) energies occupied (unoccupied) levels. We have thus employed this formalism in combination to the PBEsol⁴⁶ XC functional where U is an effective parameter $U_{\text{eff}}=U-J$.⁴⁷ We did not optimize the effective U values for each material to achieve an optimal fit (this might be done if needed in the future), but opt instead to use fixed $U=3.5$ eV for all 3d TM elements for simplicity.

III. Results

A. Examining the propensity of the symmetric structure for electronically-induced distortions

The Landau-esque symmetry breaking test perturbs a high symmetry cubic cell (here, Pm-3m with lattice parameter a_{cub}) and examines the total energy for (a) assumed equal occupations of the degenerate partners [no-OBS, such as (1/2, 1/2) for a single electron in doubly degenerate e_g level] and (b) Orbital Broken Symmetry (OBS), looking for energy lowering configurations [*e.g.* (1, 0)]. Energy differences between these configurations are provided in Table I. We see that given the opportunity for orbital broken symmetry, the compounds LaVO_3 , KFeF_3 , KCoF_3 , KCrF_3 and KCuF_3 show an energy gain $\Delta E_{\text{OBS-no/OBS}} < 0$, with a concomitant opening of the band gap, while LaTiO_3 and LaMnO_3 have $\Delta E_{\text{OBS-no/OBS}} = 0$, *i.e.* the initially imposed OBS relaxes back to configuration with equally occupied degenerate orbital, and the system stays metallic. These observations are unchanged by using another non-local functional such as HSE06^{48,49} hybrid functional method, having also a good adherence to self-interaction cancellation.

	Electronic configuration	(√2a, √2a, 2a) cubic cell (DFT+U)		Primitive cubic cell (HSE06)
		$\Delta E_{\text{OBS-no/OBS}}$ (meV/f.u)	E_g (eV)	$\Delta E_{\text{OBS-no/OBS}}$ (meV/f.u)
LaTiO₃	$d^1 (t_{2g}\uparrow^1)$	0	0	0
LaMnO₃	$d^4 (t_{2g}\uparrow^3 e_g\uparrow^1)$	0	0	0
LaVO₃	$d^2 (t_{2g}\uparrow^2)$	-297	0.42	-428
KFeF₃	$d^6 (t_{2g}\uparrow^4 e_g\uparrow^2 t_{2g}\downarrow^1)$	-655	1.78	-780
KCoF₃	$d^7 (t_{2g}\uparrow^4 e_g\uparrow^2 t_{2g}\downarrow^2)$	-726	1.90	-1071
KCrF₃	$d^4 (t_{2g}\uparrow^3 e_g\uparrow^1)$	-124	0.66	-256
KCuF₃	$d^9 (t_{2g}\uparrow^4 e_g\uparrow^2 t_{2g}\downarrow^3 e_g\downarrow^1)$	-71	0.38	-477

Table I: Detection of spontaneous electronic instability in the high symmetry cubic phase of ABX_3 perovskites. Energy differences between solutions with equal occupancy of degenerate levels (no OBS) and with the most stable orbital broken symmetries (OBS) state in meV per formula units obtained in GGA+U and HSE06 functionals (the latter uses a smaller cubic cell for computational cost reason). The lattice parameter a is fixed to a relaxed cubic cell without OBS. A FM order is assumed.

1. The emergence of orbital order from DFT total energy minimization of JTE

Once the degeneracies of the high symmetry phase are removed, one notes the creation of deterministic localization patterns of the degenerate partner components (such as $d_{x^2-y^2}$ and d_z^2) on different atomic sites. This “orbital ordering” has intrigued the community of 3d oxides^{5,45}, raising various exotic interpretations^{9,10,13,24–30}. To understand the possible unexotic, mean field total energy origins of such orbital ordering, we have investigated the energetics of different assumed orbital-arrangement: (a) electrons in the degenerate levels are initially nudged in *identical* orbitals on all nearest transition metal sites, such as a d_z^2 occupancy on all sites for a compound with a single e_g electron; (b) the electron is initially nudged in a *different* degenerate partner between nearest TM sites in the (xy) plane but on *the same* partner for TM located in the consecutive plane along the z direction, such as alternation of d_x^2 and d_y^2 in the (xy) plane with similar arrangement on the consecutive plane along z, thus forming a “columnar arrangement” and (c) the electron is initially nudged in a *different* degenerate partner between *all* nearest neighbor site, such as alternation of d_x^2 and d_y^2 in all cartesian directions, thus forming a 3D checkerboard. For a compound with 2 unpaired electrons for t_{2g} levels, case (b) and (c) necessarily require that an identical orbital has to be occupied between nearest TM sites. We thus imposed one electron in a specific t_{2g} partner on all TM sites (d_{xy} here) and then we alternate the occupancy of the remaining partners (d_{xz}/d_{yz}). After initial nudging, (intended to avoid accidental local minimum), the solution is iterated to self-consistency with full relaxation of the electronic structure but without any structural relaxation.

For all compounds displaying a spontaneous electronic instability, the lowest energy state obtained after the self-consistent field is completed *is always associated with configuration (c)* (total energies of single, columnar and checkerboard OBS states are provided in Supplementary section 1). In such a state, electrons occupy an orbital that is pointing to orthogonal directions between all nearest-neighbor transition elements, such as alternation of d_{xy}/d_{yz} orbitals for a material with a t_{2g} degeneracy, or alternation of d_y^2/d_x^2 orbitals for a material with an e_g level degeneracy as shown by our partial charge density maps of states near the Fermi level (Fig 2.a, b, d and e). This specific pattern is sometimes referred to as a G-type antiferro-orbital ordering^{13,22,50} that minimizes orbital interactions between all nearest neighbor TM site on a perfectly cubic lattice. These physical effects are usually described by the phenomenological electronic super-exchange model of Kugel and Khomskii¹⁰ (see chapter

6 of Ref.² for a detailed description of the model), that is similar to the Heisenberg Hamiltonian describing magnetic interactions. Significantly, these energy-lowering states all exhibit band gaps with respect to the cubic cell with equally occupied degenerate partners, even though no energy lowering structural relaxation has been performed (see Table I). We conclude here that in LaVO_3 , KFeF_3 , KCoF_3 , KCrF_3 and KCuF_3 , the electronic structure in the cubic cell is distorting in order to remove the orbital degeneracy, thereby producing an antiferro-orbital arrangement and opening a band gap. These compounds therefore exhibit the signatures of a Jahn-Teller effect (JTE) that is directly related to gapping.

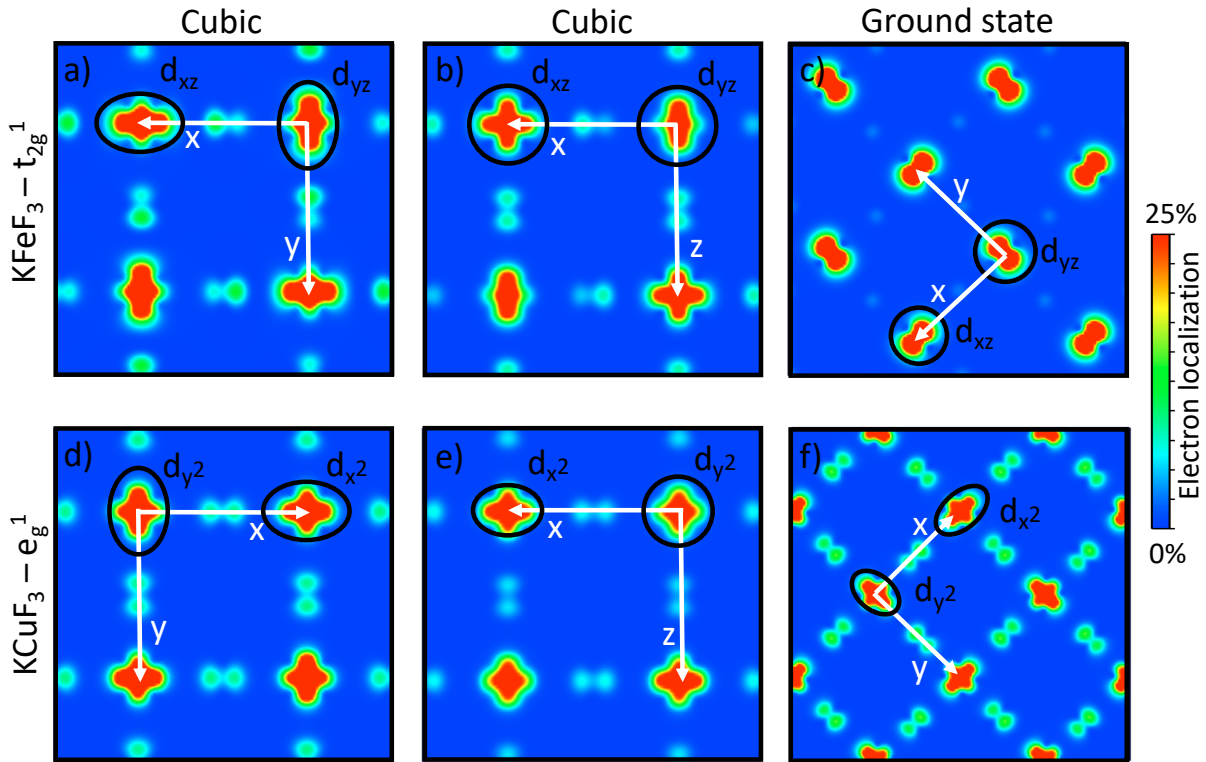


Figure 2: Orbital orderings appearing in ABX_3 materials. Wavefunction squared maps of electrons located at the top of the valence bands (latest two occupied bands) for KFeF_3 (a, b and c) and KCuF_3 (d, e and f) in their unrelaxed cubic cells (a, b, d and e) and in the fully relaxed ground state structure (c and f).

Let's note here that we previously shown that the ABO_3 perovskites with $\text{B}=3\text{d}$ ions, exhibit four distinct mechanisms of gap formation³²: (i) compounds forming closed subshells by octahedral breaking of atomic symmetry such as CaMnO_3 (t_{2g}^3) and LaFeO_3 ($t_{2g}^2e_g^3$); (ii) compounds lifting electronic degeneracies due to semiclassical, steric-induced octahedral rotations (e.g. YTiO_3 and LaMnO_3) and those retaining electronic degeneracies due to small or absent octahedral rotations (e.g. CaVO_3 and SrVO_3), insufficient to induce a gap; (iii)

compounds with two electrons in t_{2g} levels exhibiting Jahn-teller induced electronic instability causing gapping such as LaVO_3 ($t_{2g}^2e_g^0$) and (iv) compounds with unstable single local electronic occupation patterns disproportionating into a double local environment (*e.g.* CaFeO_3 and YNiO_3). Only mechanism (i) does not involve any structural motions during the gap opening but as we show here, and later in the text, gapping mechanism (iii) has contributions from both electronic and structural distortions.

1. When electronic delocalization prevents the JT effect

One might wonder at this stage why compounds with identical electronic degeneracy differ in their ability to have JT effect. For example, LaMnO_3 does not exhibit JT effect whereas KCrF_3 does; similarly, LaTiO_3 has no JT effect, whereas KFeF_3 does. To understand this, let us recall that the energy surface of a JT system⁵¹ as a function of a displacement x can be represented as $E(x) = -F_{JT}x + 1/2Kx^2$, consisting of a stabilizing electronic JT force F_{JT} associated with electronic degeneracy removal, and an opposing harmonic restoring force of the surrounding bond characterized by the force constant K . That the existence of degeneracy of partially-filled states does not automatically force a JT distortion is clear from the competition between these two terms: if the relevant (degenerate) orbitals are too hybridized/delocalized (weak F_{JT}), or the harmonic response of the bonds about to be deformed is too stiff, degeneracy will not lead to a JT distortion. To assess such tendencies, one must carry out a JT distortion theory inspecting the total (electron-electron; electron-ion and ion-ion) energy terms, not just orbital energies. This is readily done in DFT supercell theory.

To assess the difference in hybridization between fluorides and oxides, Fig. 3 shows the projected density of states of isoelectronic pairs (LaTiO_3 vs. KFeF_3 , as well as LaMnO_3 vs. KCrF_3) in the high symmetry cubic cell with equal occupancies of degenerate partners. As one can see, the fluorine-based compounds show minimal hybridizations between the B-d and X-p states, and the bandwidth associated with degenerate partners is rather narrow, thus resulting in a rather localized electronic structure and d-d like band edges. On the other hand, for oxygen-based perovskites, the hybridization between B-d and X-p states and the bandwidth associated with degenerate partners increases continuously upon adding electrons to the d levels, until reaching a ‘charge transfer insulator’ regime for LaMnO_3 – *i.e.* anion p like VBM and cation d like CBM. This thus suggests that oxides have more delocalized d states

than fluorides. Thus, in the oxides the JT force is too weak and is overcome by the restoring force but in the fluorides the JT force wins.

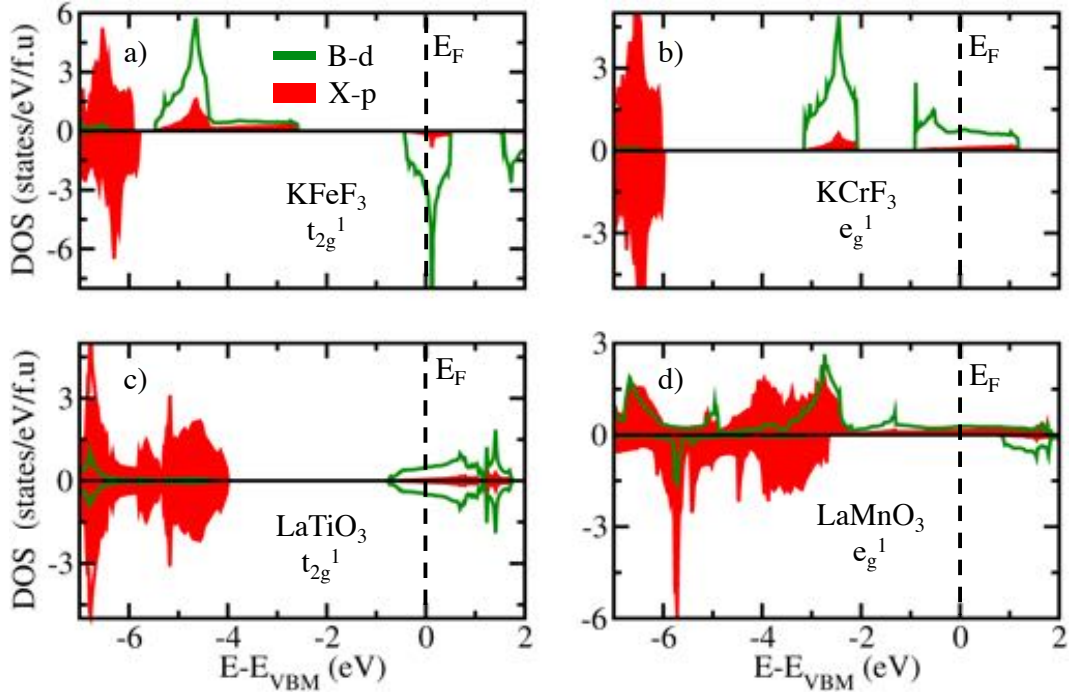


Figure 3: Electronic structure of compounds with isoelectronic degeneracies. Projected density of states on B-d (green) and X-(red) p states in materials showing a t_{2g} (KFeF₃ and LaTiO₃, panels a and c) and e_g (KCrF₃ and LaMnO₃, panels b and d) isoelectronic degeneracies in their cubic cell. The vertical line indicates the Fermi level. A simple FM order is used.

To next check how the degree of localization of degenerate orbitals induces JT displacements, we design enhanced localization in LaTiO₃ by increasing the lattice constant, *i.e.* using a (negative) hydrostatic pressure. Starting from this new cubic cell in which the bandwidth of the t_{2g} degenerate partners is reduced by 0.5 eV *wrt* the unperturbed cubic cell, we again nudge the Ti³⁺ electron to specific t_{2g} partners (see Supplementary Section 2). LaTiO₃ now develops a small electronic instability ($\Delta E_{\text{OBS-no OBS}} = -6$ meV/f.u) producing an antiferro-orbital occupancy between all nearest neighbor Ti³⁺ sites and opening a band gap of 0.1 eV. Therefore, upon decreasing B, d – X, p hybridizations and the t_{2g} levels bandwidth, LaTiO₃ undergoes a Jahn-Teller effect.

We conclude that delocalized degenerate states can prevent an electronic instability and the ensuing Jahn-Teller effect despite the presence of orbital degenerate states.

4. Trends in JT energies with orbital occupancy

Although LaVO_3 exhibits similar B, d – X, p hybridizations as LaTiO_3 , the former compound LaVO_3 possesses a robust electronic instability in the cubic cell (energy lowering of 297 meV), while LaTiO_3 has zero stabilization energy. As illustrated in Table I, this reflects the fact that the JT force is larger in systems with higher orbital occupancy – LaVO_3 with two electrons $t_{2g}^{\uparrow 2}$ relative to LaTiO_3 with just one $t_{2g}^{\uparrow 1}$. Similarly, the energy gain associated with breaking orbital degeneracies increases when going from t_{2g}^1 in KFeF_3 to a t_{2g}^2 in KCoF_3 . In general, we expect that triply degenerate states occupied by 2 electrons to have the greatest JT instability.

Having established the trends in *energetics* for electronically -induced JTD we next discuss the nature of the JT *displacements*.

B. The Q_2^- octahedral deformation mode is a Jahn-Teller distortion

1. Electronically unstable cubic structures develop the Q_2^- octahedral deformation upon relaxation

While literature often ascribe Q_2^+ and Q_2^- modes to a JT effect ^{2,5}, we inspect here the type of distortion forced by the spontaneous electronic instability in the hypothetical cubic structure of LaVO_3 , KFeF_3 , KCoF_3 , KCrF_3 and KCuF_3 . To that end, we allow these systems to change their structures by fully developing energy lowering displacements. Application of structural relaxation techniques (following quantum mechanical forces to zero force configurations) reveals all these systems develop specifically the anti-*phase* Q_2^- octahedral deformation that we therefore consider as the fingerprint of JT effect in these systems. We tested the Q_2^+ octahedral deformation mode but this octahedral deformation mode produces lower energy gains than the Q_2^- mode (see Supplementary Section 3).

Symmetry adapted mode analysis of the relaxed DFT structures (starting from experimentally observed structures and magnetic orders) are presented in Table II. One can appreciate the development of the specific Q_2^- mode by the presence of shifted single well potential energy surface associated with the Q_2^- mode starting from a cubic cell, signaling the presence of a Jahn-Teller force F_{JT} (see Supplementary Section 4). Note that the shifted single wells are independent of the spin order (FM and AFM orders yield similar results), and thus

the magnetic order at low temperature is a consequence of the specific orbital-orderings forced by the electronic instability. The significance of the development of this specific Q_2^- mode (Figure 1.d) is that it is characterized by *opposite* octahedral deformations between nearest sites, and is thus able to accommodate and amplifies the incipient orbital-orderings (Fig 2.c and f): B-X bonds expand and contract in the plane defined by the alternating directions of the occupied orbitals.

2. Theory vs. experimental observation for the Q_2^- octahedral deformation mode

The predicted specific symmetry of the Q_2^- mode is precisely what is needed to explain the cubic to tetragonal I_4/mcm structural transition in $KCrF_3$ and $KCuF_3$ (observed at $T=973$ K and 800 K^{52,53}, respectively), and of the $Pbnm$ to $P2_1/b$ structural transition observed in RVO_3 compounds ($R=Lu-La, Y$)^{22,54}. Table II summarizes the calculated vs. experimental values of the *amplitudes* of the Q_2^- displacements, showing very good agreement.

	t factor	Magnetic order	Space Group	$Q_2^+ (M_3^+)$ Calculated (Exp.)	$Q_2^- (R_3^-)$ Calculated (Exp.)
LaTiO₃	0.93	AFM-G	Pbnm	0.040 (0.041 ⁵⁵)	-
LaMnO₃	0.94	AFM-A	Pbnm	0.324 (0.357 ²¹)	-
LaVO₃	0.95	AFM-C	$P2_1/b$	0.005 (0.009 ⁵⁶)	0.093 (0.079 ⁵⁶)
			Pbnm	0.078 (0.090 ⁵⁷)	-
KFeF₃	1.00	AFM-G	I_2/a	-	0.104 (-)
KCoF₃	1.01	AFM-G	P-1	-	0.003 (-)
KCrF₃	0.99	AFM-A	I_2/m	-	0.336 (0.316 ¹⁹)
			I_4/mcm	-	0.300 (0.299 ¹⁹)
KCuF₃	1.03	AFM-A	I_4/mcm	-	0.335 (0.355 ²⁰)

Table II: Amplitudes associated with structurally distorted octahedra in the ground state of ABX_3 perovskites. Amplitudes of distortions (in Å) associated with the Q_2^+ and Q_2^- modes (irreducible representations M_3^+ and R_3^- respectively) distorting octahedra of the optimized structures starting from a cubic cell with the A cation located at the corner of the cell.

Experimental values extracted from structures available in literature are provided in parenthesis. The Goldschmidt t factor is also reported, as well as the magnetic state observed experimentally at low temperature and assumed in the simulation for the relaxation of the ground states.

2. The atomic displacements yielding the JTD are strongly coupled to octahedral rotations and to the electronic configuration

Along with the presence of JT like atomic displacements in cubic cells, ABX_3 compounds are also characterized by the spontaneous appearance of octahedral rotations, associated with pure steric effects, (also called ‘chemical pressure’ effects). The propensity for octahedral rotations is correlated with the 1926 Goldschmidt tolerance factor given by $t = \frac{r_B + r_O}{\sqrt{2}(r_A + r_O)}$ where r are atomic radii that quantifies the ion size mismatch. Here, $t=1$ would represent a perfect packing of ions in the cubic cell without rotations, whereas $t < 1$ is correlated with rotations. Among the compounds that display a JTD, $KCrF_3$ and $LaVO_3$ exhibit octahedral rotations at low temperature, being either a single anti-phase rotation in $KCrF_3$ or a combination of two anti-phase and one in-phase rotations in $LaVO_3$. The most basic question is then *how does these rotations couple with the JT effect: do electronic and steric effects cooperate or compete?*

In $KCrF_3$, the energy gain associated with the ϕ_z^- anti-phase octahedra rotation is one order of magnitude smaller ($\Delta E_{rot} = -32$ meV/f.u) than the energy gain produced by the electronic instability ($\Delta E = -124$ meV/f.u), further amplified by the JT distortion ($\Delta E_{JTD} = -140$ meV/f.u). Thus, the rotation appears at a temperature far below the JT effect. This is indeed observed experimentally: the material transits from a tetragonal to a I_2/m monoclinic cell at $T = 250$ K, a temperature much lower than that of the JT effect ($T = 973$ K). In the I_2/m symmetry, the octahedra rotation and the JT distortion have orthogonal atomic displacements patterns: X_6 groups rotate around the z axis – F motions along the x and y axes – while the JT distortion propagates along the y axis – F motions along the x and z axes. Such a peculiar orientation of propagation axes minimizes the electronic super-exchange at the core of the JT effect (see supplementary Section 5) and enables by symmetry an extra component to the JT distortion in which apices X anions move inward/outward the B cation, therefore very slightly modifying orbital shapes. However, unlike previous statements

involving strong correlations effects, Slater super-exchange, or covalent effects⁵⁸ for explaining the tetragonal to monoclinic transition, it is driven by nothing else than a steric effect (a NM simulation also provides a stabilization of the rotation mode). Let's note that the different orientations of occupied orbitals between the tetragonal (alternation of d_x^2 and d_y^2 orbitals) and monoclinic (alternation of d_z^2 and d_y^2 orbitals) cells simply originate from an arbitrary choice of different crystallographic parameters between the two symmetries.

The situation is somehow different in LaVO_3 : the X_6 rotations produce energy gains ($\Delta E \approx -530$ and -300 meV/f.u for ϕ_{xy}^- and ϕ_z^+ rotations, respectively) larger than the electronic instability associated with the t_{2g}^2 electronic configuration ($\Delta E \approx -297$ meV/f.u, see Table II) yielding the JTD. The rotations therefore condense first and already produce an insulating orthorhombic Pbnm symmetry ($E_g = 1.47$ eV with the AFMC order). Within this intermediate phase, we do observe a very narrow electronic instability willing to produce a G-type antiferro-orbital ordering ($\Delta E = -0.5$ meV/f.u with AFMC and FM orders) that forces the JTD ($\Delta E = -16$ meV/f.u).

Surprisingly, these rotations strongly couple with the electronic instability yielding the JT distortion in LaVO_3 (see Supplementary Section 6): (i) minimization of electronic super-exchange forces the in-phase rotation ϕ_z^+ and the JT distortion to propagate along the same axis, z here, and (ii) from large to moderate ϕ_z^+ rotation amplitude, the strength of the electronic instability increases and then it decreases when going to small X_6 rotations. This latter behavior originates from three opposite facts: the ϕ_z^+ rotation split the t_{2g} levels by pushing to lower energies the d_{xy} orbital due to point group symmetry lowering from O_h to D_{4h} ; (ii) thereby reducing the bandwidth associated with degenerate partners but (iii) at the same time they increase hybridization of V, d levels with O, p levels. Such an observation is strictly compatible with the rare-earth dependence of the Q_2^- structural/JTE temperature transition in RVO_3 compounds²².

We conclude here that JT distortion and rotations can either compete or cooperate depending on the involved degenerate states, thus offering a knob to tune the JT effect in ABX_3 materials.

C. The Q_2^+ motion in LaTiO_3 and LaMnO_3 is a consequence of classic octahedral rotations and tilting, not a quantal JT effect

Consistent with the absence of electronic instabilities in the high symmetry Pm-3m cubic cell of LaTiO_3 and LaMnO_3 , we find that the Q_2^+ or Q_2^- octahedra deformation are associated with a single well energy potential and are further unable to open a band gap (see figure 4.a and b). Such observations were already raised by Lee *et al* for LaMnO_3 in Ref.⁵⁹. This means that, although a sizable Q_2^+ octahedra deformations mode appears in the ground state structure of LaTiO_3 and LaMnO_3 , the Q_2^+ mode does not spontaneously lift orbital degeneracies and produce the metal-to-insulator transition.

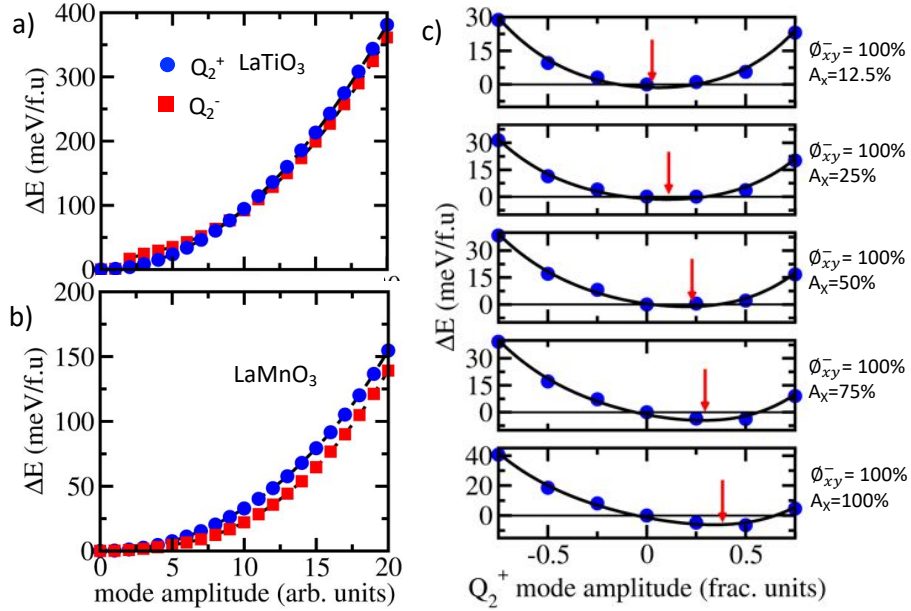


Figure 4: Induced Q_2^+ motions through lattice mode couplings. a and b) Energy versus Q_2^+ (filled blue circles) and Q_2^- (filled red squares) mode amplitudes (arbitrary units) in LaTiO_3 (a) and LaMnO_3 (b) using a FM order starting from a cubic cell. c) Energy versus Q_2^+ mode amplitude at fixed amplitude of ϕ_{xy}^- and A_x in LaMnO_3 using a FM order. 1 (100%) represents the amplitude appearing in the ground state.

Nevertheless, these compounds develop two anti-phase and one in-phase X_6 rotations (see t factor in Table II) that allow a specific lattice mode coupling between the Q_2^+ mode, the antiphase rotation ϕ_{xy}^- and an antipolar motion A_x (sketched in Fig 1. of Ref.²⁷) of the form $F \propto \phi_{xy}^- A_x Q_2^+$ in the free energy expansion as identified in Ref.¹³, the appearance of finite

amplitudes of ϕ_{xy}^- and the A_x modes automatically forces finite amplitudes of the Q_2^+ mode in the material in order to lower the total energy as we see in Fig.4.c for LaMnO_3 (a similar conclusion is raised for LaTiO_3 but is not shown). Although the dependency of the Q_2^+ mode with rotations amplitude in LaMnO_3 was already shown in Ref.⁵⁹, we show that the Q_2^+ is nothing else than a consequence of ABX_3 distortions originating from pure steric effects captured by the 1926 Goldschmidt tolerance factor³. By performing a parallel with improper ferroelectrics^{60,61}, the Q_2^+ mode has an improper appearance, being a simple consequential of a specific octahedra rotations pattern, namely a combination of two anti-phase and one in-phase rotations. This Q_2^+ motion should not be confused with a JTD associated with an electronic instability, in contrast to usual statements^{9,21,29,62,63}.

1. The appearance of an Q_2^+ mode is not a statement of strong dynamical correlation effects

Leonov *et al*²⁹ highlighted the importance of dynamical correlations on the stabilization of the Q_2^+ mode in LaMnO_3 . They plotted the potential energy surface as a function of the Q_2^+ mode amplitude with Dynamical Mean Field Theory (DMFT) simulations starting from a cell with rotations and the A_x mode, explaining that “*in the calculation we change only the parameter ∂_{JT} ... and keep the value of the MnO_6 octahedron tilting and rotation fixed*”. As can be seen, their DMFT results agrees closely with our DFT result, suggesting that in this case, treating dynamical electronic correlations does not bring any new features to the understanding of the octahedra deformation in ABX_3 materials.

2. The origin of the improper Q_2^+ motion in LaMnO_3

Our first-principles results demonstrate that the Q_2^+ mode is a simple consequence of octahedra rotations, but one wonders if one can extract experimental evidences of this phenomena. At high temperature, LaMnO_3 adopts a rhombohedral R-3c phase that is characterized by an anti-phase rotation ϕ_{xyz}^- around all cartesian axes and in which no octahedral deformation nor related phenomena such as an orbital-ordering are reported^{21,64}. This is compatible with our models since (i) no electronic instability yielding a Q_2^- JTD mode is identified in LaMnO_3 and (ii) such X_6 octahedra tilt pattern does not allow A_x and Q_2^+ modes to develop by symmetry. Once LaMnO_3 transforms to the Pbnm cell around 750 K, one

observes that experimental structures at various temperature taken from Ref.²¹ develop an A_x distortion whose amplitude increases with decreasing temperature while ϕ_{xy}^- is not temperature dependent. Upon enlargement of the A_x mode amplitude on cooling, a substantial Q_2^+ mode appears in the material (See supplementary Section 7 for symmetry adapted modes of these structures). It thus confirms the “improper appearance” of the Q_2^+ octahedra distortion mode.

IV. Conclusions

We have explained the modalities enabling a Jahn-Teller effect in ABX_3 perovskites and identified its signature: strongly localized electronic states or a t_{2g}^2 electronic configuration are the key factor for a spontaneous electronic instability to produce a Jahn-Teller distortion with a specific octahedra deformation pattern that is experimentally detectable and detected. In materials with larger anions p and B cations d states hybridizations, there is no electronic instability willing to break orbital degeneracies and the observed octahedra deformation has a distinct symmetry that is pushed by lattice mode couplings with rotations. Our work thus provides a single theory explaining the Jahn-Teller effect and its specific signatures and reconcile the numerous experimental results of ABX_3 materials studied to date. Last but not least, our results settle the fact that dynamical correlations, and the Mott-Hubbard model, are absolutely not an essential aspect of the physics of ABX_3 materials showing insulating states despite the presence of degenerate states in the parent cubic cell, thereby defining DFT as a sufficient platform to study the physics of ABX_3 materials.

Method: DFT calculations are performed with the VASP package^{43,65} and electrons are nudged using the modified VASP routine⁴⁴. We used PAW potentials with the outer 4s, 4p and 3d B cation electrons explicitly treated in the simulations. $6*6*4$ k-point mesh was used for the relaxation of the ($\sqrt{2}a, \sqrt{2}a, 2a$) cubic cells, increased to $8*8*6$ for plotting energy potential surfaces and seeking for OBS, accompanied by an energy cut-off of 500 eV.

Acknowledgments: This work of JV has been supported by the European Research Council (ERC) Consolidator grant MINT under the Contract No. 615759. Calculations took advantages of the Occigen machines through the DARI project EPOC A0020910084 and of the DECI resource FIONN in Ireland at ICHEC through the PRACE project FiPSCO. The work of AZ was supported by Department of Energy, Office of Science, Basic Energy Science, MSE division under Grant No. DE-FG02-13ER46959 to CU Boulder. JV acknowledges support from A. Ralph at ICHEC supercomputers.

References

1. (Eds.), H. K. D. R. Y. H. B. *The Jahn-Teller Effect Fundamentals and Implications for Physics and Chemistry*. (2009).
2. Khomskii, D. I. *Transition Metal Compounds*. Cambridge University Press **1**, (2014).
3. Goldschmidt, V. M. Die gesetze der krystallochemie. *Naturwissenschaften* **14**, 477–485 (1926).
4. Tokura, Y. & Nagaosa, N. Orbital physics in transition-metal oxides. *Science* (80-.). **288**, 462–468 (2000).
5. Goodenough, J. B. Jahn-Teller Phenomena in Solids. *Annu. Rev. Mater. Sci.* **28**, 1–27 (1998).
6. Jahn, H. A. & Teller, E. Stability of polyatomic molecules in degenerate electronic states. I. Orbital degeneracy. *Proc. R. Soc. London Ser. A - Math. Phys. Sci.* **161**, 220–235 (1937).
7. Baldini, M., Struzhkin, V. V., Goncharov, A. F., Postorino, P. & Mao, W. L. Persistence of Jahn-Teller distortion up to the insulator to metal transition in LaMnO₃. *Phys. Rev. Lett.* **106**, 064402 (2011).
8. Binggeli, N. & Altarelli, M. Orbital ordering, Jahn-Teller distortion, and resonant x-ray scattering in KCuF₃. **085117**, 1–10 (2004).
9. Pavarini, E. & Koch, E. Origin of jahn-teller distortion and orbital order in LaMnO₃. *Phys. Rev. Lett.* **104**, 086402 (2010).
10. Kugel, K. I. & Khomskii, D. I. Crystal structure and magnetic properties of substances with orbital degeneracy. *Sov. Phys. JETP* **64**, 1429–1439 (1973).
11. Kugel, K. I. & Khomskii, D. I. The Jahn-Teller effect and magnetism : transition metal compounds The Jahn-Teller effect and magnetism : transition metal compounds.

- (1982).
12. Ren, Y. *et al.* Temperature-induced magnetization reversal in a YVO₃ single crystal. *Nature* **396**, 441–444 (1998).
 13. Varignon, J., Bristowe, N. C., Bousquet, E. & Ghosez, P. Coupling and electrical control of structural, orbital and magnetic orders in perovskites. *Sci. Rep.* **5**, 15364 (2015).
 14. Varignon, J., Bristowe, N. C. & Ghosez, P. Electric Field Control of Jahn-Teller Distortions in Bulk Perovskites. *Phys. Rev. Lett.* **116**, 57602 (2016).
 15. Stroppa, A., Barone, P., Jain, P., Perez-Mato, J. M. & Picozzi, S. Hybrid Improper Ferroelectricity in a Multiferroic and Magnetoelectric Metal-Organic Framework. *Adv. Mater.* **25**, 2284 (2013).
 16. Stroppa, A. *et al.* Electric control of magnetization and interplay between orbital ordering and ferroelectricity in a multiferroic metal-organic framework. *Angew. Chemie - Int. Ed.* **50**, 5847–5850 (2011).
 17. Chaloupka, J. & Khaliullin, G. Orbital order and possible superconductivity in LaNiO₃/LaMO₃ superlattices. *Phys. Rev. Lett.* **100**, 16404 (2008).
 18. Kumar, D. *et al.* Magnetism tailored by mechanical strain engineering in PrVO₃ thin films. **224405**, 1–11 (2019).
 19. Margadonna, S. & Karotsis, G. Cooperative Jahn-Teller Distortion, Phase Transitions, and Weak Ferromagnetism in the KCrF₃ Perovskite. *J. Am. Chem. Soc.* **128**, 16436–16437 (2006).
 20. Okazaki, A. & Suemune, Y. The Crystal Structure of KCuF₃. *J. Phys. Soc. Jpn* **16**, 176 (1961).
 21. Rodriguez-Carvajal, J., Hennion, M., Moussa, F. & Moudden, A. H. Neutron-diffraction study of the Jahn-Teller transition in stoichiometric LaMnO₃. *Phys. Rev. B.* **57**, 3189–3192 (1998).
 22. Sage, M. H., Blake, G. R., Marquina, C. & Palstra, T. T. M. Competing orbital ordering in RVO₃ compounds: High-resolution x-ray diffraction and thermal expansion. *Phys. Rev. B* **76**, 195102 (2007).
 23. Yang, Y., Ren, W., Stengel, M., Yan, X. H. & Bellaiche, L. Revisiting properties of ferroelectric and multiferroic thin films under tensile strain from first principles. *Phys. Rev. Lett.* **109**, 57602 (2012).
 24. Kugel, K. I. & Khomskii, D. I. Crystal-structure and magnetic properties of substances

- with orbital degeneracy. *Zh. Eksp. Teor. Fiz* **64**, 1429–1439 (1973).
25. Pavarini, E., Koch, E., Lichtenstein, A. I. & Flesch, A. Origin of Orbital Order in KCuF_3 and LaMnO_3 .
 26. Pavarini, E., Koch, E. & Lichtenstein, A. I. Mechanism for Orbital Ordering in KCuF_3 . *Phys. Rev. Lett.* **101**, 266405 (2008).
 27. Varignon, J., Grisolia, M. N., Preziosi, D., Ghosez, P. & Bibes, M. Origin of the orbital and spin ordering in rare-earth titanates. *Phys. Rev. B* **96**, 235106 (2017).
 28. Carpenter, M. A. & Howard, C. J. Symmetry rules and strain/order-parameter relationships for coupling between octahedral tilting and cooperative Jahn-Teller transitions in ABX_3 perovskites. I. Theory. *Acta Crystallogr. Sect. B Struct. Sci.* **65**, 134–146 (2009).
 29. Leonov, I., Korotin, D., Binggeli, N., Anisimov, V. I. & Vollhardt, D. Computation of correlation-induced atomic displacements and structural transformations in paramagnetic KCuF_3 and LaMnO_3 . *Phys. Rev. B* **81**, 075109 (2010).
 30. Leonov, I. *et al.* Structural relaxation due to electronic correlations in the paramagnetic insulator KCuF_3 . *Phys. Rev. Lett.* **101**, 096405 (2008).
 31. Varignon, J., Bibes, M. & Zunger, A. Mott gapping in 3d ABO_3 perovskites without Mott-Hubbard interelectronic U. *ArXiv* 1901.00425 (2019).
 32. Varignon, J., Bibes, M. & Zunger, A. Origin of band gaps in 3d perovskite oxides. *Nat. Commun.* **10**, 1658 (2019).
 33. Xu, S., Shen, X., Hallman, K. A., Haglund, R. F. & Pantelides, S. T. Unified band-theoretic description of structural, electronic, and magnetic properties of vanadium dioxide phases. *Phys. Rev. B* **95**, 125105 (2017).
 34. Trimarchi, G., Wang, Z. & Zunger, A. Polymorphous band structure model of gapping in the antiferromagnetic and paramagnetic phases of the Mott insulators MnO , FeO , CoO , and NiO . *Phys. Rev. B* **97**, 035107 (2018).
 35. Dalpian, G. M., Liu, Q., Varignon, J., Bibes, M. & Zunger, A. Bond disproportionation, charge self-regulation, and ligand holes in s- p and in d-electron ABX_3 perovskites by density functional theory. *Phys. Rev. B* **98**, 075135 (2018).
 36. Furness, J. W. *et al.* An accurate first-principles treatment of doping-dependent electronic structure of high-temperature cuprate superconductors. *Commun. Phys.* **1**, 11 (2018).

37. Lane, C. *et al.* Antiferromagnetic ground state of La₂CuO₄: A parameter-free ab initio description. *Phys. Rev. B* **98**, 125140 (2018).
38. Liu, Q. *et al.* Electron Doping of Proposed Kagome Quantum Spin Liquid Produces Localized States in the Band Gap. *Phys. Rev. Lett.* **121**, 186402 (2018).
39. Liu, Q., Dalpian, G. M. & Zunger, A. Antidoping in Insulators and Semiconductors Having Intermediate Bands with Trapped Carriers. *Phys. Rev. Lett.* **122**, 106403 (2019).
40. Perez-Mato, J. M., Orobengoa, D. & Aroyo, M. I. Mode crystallography of distorted structures. *Acta Crystallogr. Sect. A Found. Crystallogr.* **66**, 558–590 (2010).
41. Orobengoa, D., Capillas, C., Aroyo, I. & Perez, J. M. AMPLIMODES : Symmetry mode analysis on the Bilbao Crystallographic Server research papers. *J. Appl. Crystallogr.* **42**, 820 (2009).
42. Kresse, G. & Haffner, J. No Title. *Phys. Rev. B* **47**, 558 (1993).
43. Kresse, G. & Furthmüller, J. Efficiency of ab-initio total energy calculations for metals and semiconductors using a plane-wave basis set. *Comput. Mater. Sci.* **6**, 15 (1996).
44. Allen, J. P. & Watson, G. W. Occupation matrix control of d- and f-electron localisations using DFT + U. *Phys. Chem. Chem. Phys.* **16**, 21016 (2014).
45. Kugel', K. I. & Khomskii, D. I. The Jahn-Teller effect and magnetism: transition metal compounds. *Sov. Phys. Usp.* **25**, 231 (1982).
46. Perdew, J. P. *et al.* Restoring the Density-Gradient Expansion for Exchange in Solids and Surfaces. *Phys. Rev. Lett.* **100**, 136406 (2008).
47. Dudarev, S. L., Savrasov, S. Y., Humphreys, C. J. & Sutton, a. P. Electron-energy-loss spectra and the structural stability of nickel oxide: An LSDA+U study. *Phys. Rev. B* **57**, 1505–1509 (1998).
48. Heyd, J., Scuseria, G. E. & Ernzerhof, M. Hybrid functionals based on a screened Coulomb potential. *J. Chem. Phys.* **118**, 8207–8215 (2003).
49. Krukau, A. V., Vydrov, O. A., Izmaylov, A. F. & Scuseria, G. E. Influence of the exchange screening parameter on the performance of screened hybrid functionals. *J. Chem. Phys.* **125**, 224106 (2006).
50. Miyasaka, S., Fujioka, J., Iwama, M., Okimoto, Y. & Tokura, Y. Raman study of spin and orbital order and excitations in perovskite-type RVO₃ (R=La, Nd, and Y). *Phys. Rev. B - Condens. Matter Mater. Phys.* **73**, 224436 (2006).

51. Baraff, G. A., Kane, E. O. & Schlüter, M. Theory of the silicon vacancy: An Anderson negative-U system. *Phys. Rev. B* **21**, 5662–5686 (1980).
52. Margadonna, S. & Karotsis, G. High temperature orbital order melting in KCrF₃ perovskite. *J. Mater. Chem.* **17**, 2013–2020 (2007).
53. Paolasini, L., Caciuffo, R., Sollier, A., Ghigna, P. & Altarelli, M. Coupling between Spin and Orbital Degrees of Freedom in KCuF₃. *Phys. Rev. Lett.* **88**, 106403 (2002).
54. Miyasaka, S., Okimoto, Y., Iwama, M. & Tokura, Y. Spin-orbital phase diagram of perovskite-type RVO₃ (R= rare-earth ion or Y). *Phys. Rev. B* **68**, 100406 (2003).
55. Cwik, M. *et al.* Crystal and magnetic structure of LaTiO₃: Evidence for nondegenerate t_{2g} orbitals. *Phys. Rev. B* **68**, 060401 (2003).
56. Bordet, P. *et al.* Structural aspects of the crystallographic-magnetic transition in LaVO₃ around 140 K. *J. Solid State Chem.* **106**, 253 (1993).
57. Seim, H. & Fjellvag, H. Non-Stoichiometric LaVO₃. I. Synthesis and Physical Properties. *Acta Chem. Scand.* **52**, 1096–1103 (1998).
58. Autieri, C., Koch, E. & Pavarini, E. Mechanism of structural phase transitions in KCrF₃. *Phys. Rev. B* **89**, 155109 (2014).
59. Lee, J. H., Delaney, K. T., Bousquet, E., Spaldin, N. A. & Rabe, K. M. Strong coupling of Jahn-Teller distortion to oxygen-octahedron rotation and functional properties in epitaxially strained orthorhombic LaMnO₃. *Phys. Rev. B* **88**, 174426 (2013).
60. Fennie, C. J. & Rabe, K. M. Ferroelectric transition in YMnO₃ from first principles. *Phys. Rev. B* **72**, 100103(R) (2005).
61. Bousquet, E. *et al.* Improper ferroelectricity in perovskite oxide artificial superlattices. *Nature* **452**, 732–736 (2008).
62. Hemberger, J. *et al.* Evidence for Jahn-Teller Distortions at the Antiferromagnetic Transition in LaTiO₃. *Phys Rev Lett.* **91**, 066403 (2003).
63. Cwik, M. *et al.* Crystal and magnetic structure of LaTiO₃: Evidence for nondegenerate t_{2g} orbitals. *Phys. Rev. B* **68**, 060401 (2003).
64. Qiu, X., Proffen, T., Mitchell, J. F. & Billinge, S. J. L. Orbital correlations in the pseudocubic O and rhombohedral R phases of LaMnO₃. *Phys. Rev. Lett.* **94**, 1–4 (2005).
65. Kresse, G. & Hafner, J. Ab initio molecular dynamics for liquid metals. *Phys. Rev. B* **47**, 558–561 (1993).

